

Supplementary Information

The "Smart" Valve for Micro Flow-Velocity Regulation Based on the "Interfacial Barrier" Effect of Wettability-Patterned Surfaces

Litao Chen,^a Yimin Luo,^{*a} Jincheng Liu,^a Boran Hao,^a Shushen Lyu,^a
Zhuangzhu Luo^{a*}

^aSchool of Materials, Sun Yat-Sen University, Shenzhen 518107, P. R. China

*Corresponding authors: luoym55@mail.sysu.edu.cn;
luozhuzhu@mail.sysu.edu.cn

Methods

Materials and Coating Preparation. The bare aluminum substrate was sequentially polished with 800# sandpaper, then ultrasonically cleaned in acetone for 5 minutes, and dried to obtain Surf 0. The high surface energy polymer (PEG) filler was ground and ultrasonically dispersed in an aqueous phase to obtain a PEG solution, which was then mixed with polyphenylene sulfide (PPS) in a specific volume ratio. Under an air pressure of 0.1~0.2 MPa, the coating precursor was atomized using a spray gun (Yantian W-101-131 G) to form a wet coating film. The film was heated to 150°C within 10 minutes and held for 30 minutes, then further heated to 390°C over 60 minutes and held for another 60 minutes. The sample was cooled in the furnace to 120°C, after which it was removed to complete the curing process, resulting in the Surf 1 coating. The commercially available PTFE powder with low surface energy was dispersed in a mixed solvent (distilled water/ethanol/isobutyl alcohol in a volume ratio of 2:5:1), along with 10 wt% nonionic surfactant (octylphenol polyoxyethylene ether: C₈H₁₇-Ph-O(C₂H₄O)_nH, n≈10), and 0.5M (NH₄)₂CO₃ solution with ultrasonic stirring for 30 min, which gave the PTFE emulsion (O/W). PPS resin was selected as the binder. The binder was then mixed into the PTFE emulsion and dispersed for 10 minutes to form the coating precursor. The superhydrophobic coatings were prepared by spraying the coating precursor and curing at 150°C for 0.5 hours and 390°C for 1.5 hours.

Subsequently, the Surf 2 coating was naturally cooled in air to room temperature. The porous structure and the enrichment of low surface energy material ($-CF_3$) on the surface resulted in a surface WCA of 150.82° .

Characterization. The roughness of the coatings was measured using a TR100 surface roughness tester, while the thickness of the coatings was determined using a TT260 microprocessor coating thickness gauge (Beijing Jintai Times Technology Co. Ltd, Beijing, China). The thickness of the coatings on various substrates ranged from 20 to 30 μm . The static contact angle (WCA) of 5 μL distilled water droplets on the coatings was measured using a contact angle measurement apparatus (DSA-100, KRÜSS GmbH, Hamburg, Germany). The microstructures of the coating surfaces were examined using scanning electron microscopy (MIRA3, TESCAN).

Measurement of Flow Behavior. The water flow experimental system for wettability-patterned surfaces primarily consisted of a peristaltic pump for droplet transportation, a droplet generator with a needle, wall surface samples fixed at a 45° inclination angle, an adjustable-angle sample holder, and a position-adjustable platform to support the impacted surface. Image acquisition was mainly conducted using digital cameras for general observation, while high-speed cameras provided supplementary data for detailed motion capture. The setup was illuminated by a flicker-free lamp to ensure consistent lighting, and a computer was used to record and store the captured images and videos. During the experiment, the wall surface samples were fixed at a 45° inclination to simulate inclined flow conditions, and the position-adjustable platform ensured precise alignment of the impacted surface. Digital cameras served as the primary tool for capturing flow behavior, while high-speed cameras (with a frame rate of up to 2000 frames per second) were utilized when detailed dynamic processes needed to be observed. The captured data were processed and analyzed using software such as ImageJ and Origin, ensuring a comprehensive evaluation of flow behavior on wettability-patterned surfaces.

Measurement of Droplet Impact Behavior. The experimental system for single droplet impact on wettability-patterned surfaces included a peristaltic pump for droplet transportation, a droplet generator with a needle, wall surface samples, a high-speed

camera for image acquisition, a flicker-free lamp for consistent illumination, and a computer for recording and storing the captured images. The high-speed camera, operating at up to 2000 frames per second, ensured precise observation of droplet impact dynamics. The flicker-free lamp provided stable lighting conditions, enhancing image quality for detailed analysis. Data captured during the experiment were processed using software such as ImageJ and Origin to comprehensively study droplet impact behavior.

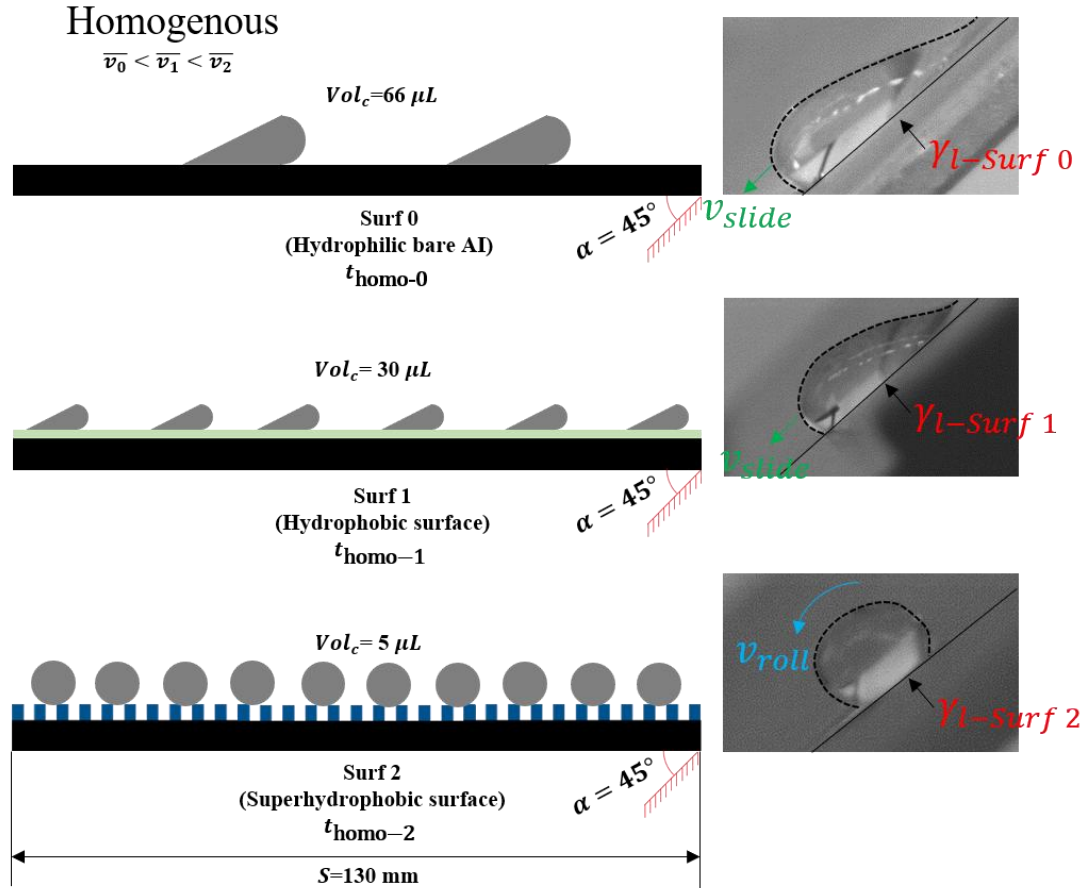


Fig. S1 Water flow on homogeneous wettability surfaces.

Continuous water flow on a homogeneous wettability surface inclined at 45° forms a discontinuous sequence of droplets. As shown in Fig. S3, water slides on the bare aluminum substrate (Surf 0) and the hydrophobic surface (Surf 1) in a spindle-shape. For the same flow distance ($S = 130 \text{ mm}$), the average flow velocities are $\bar{v}_0 = 0.057 \text{ m/s}$ and $\bar{v}_1 = 0.083 \text{ m/s}$, with corresponding flow times of $T_0 = 2270 \text{ ms}$ and $T_1 = 1570 \text{ ms}$, respectively. On the superhydrophobic surface (Surf 2), water rolls in a ball-shape, and the average flow velocity significantly increases to $\bar{v}_2 = 0.325 \text{ m/s}$, which is six times higher than on the bare aluminum substrate and four times higher than on the hydrophobic surface, with the flow time reduced to $T_2 = 400 \text{ ms}$. Comparing the bare aluminum substrate and the hydrophobic surface, the increase in hydrophobicity corresponds to an increase in average flow velocity. Comparing the hydrophobic surface with the superhydrophobic surface, the presence of air pockets on the superhydrophobic surface transforms flow mode from sliding to rolling, resulting

in a significant increase in average flow velocity. Overall, as surface hydrophobicity increases, the flow mode transitions from sliding (spindle-shape) to rolling (ball-shape). This dynamic wetting behavior greatly enhances the average flow velocity and reduces the flow time.

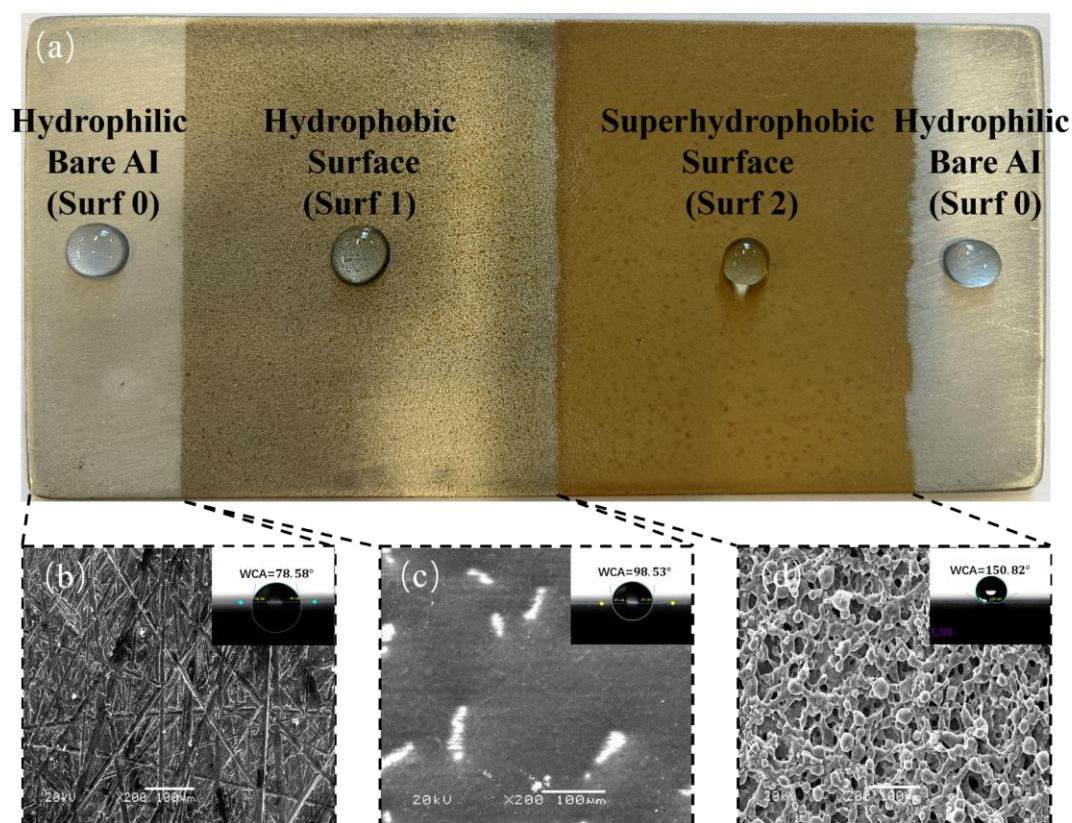


Fig. S2 Optical image (a) and SEM images (b-d) of a wettability-patterned surface.

Building on the team's earlier work, three surfaces with distinct characteristics were selected: a bare aluminum substrate (Surf 0), a dense hydrophobic coating (Surf 1), and a lotus-leaf-inspired superhydrophobic coating (Surf 2). Wettability-patterned surfaces were fabricated using a sequential spray-coating process (Fig. S1a). Surf 0 (Fig. S1b) exhibits a water contact angle (WCA) of 78.58° , with droplets in the Wenzel state, indicating no air pockets at the solid-liquid interface. The surface roughness (R_a) is approximately $1\ \mu\text{m}$, making it nearly smooth. Surf 1 (Fig. S1c) has a WCA of 98.53° , with droplets also in the Wenzel state and no air pockets at the solid-liquid interface. Its surface roughness is around $3\ \mu\text{m}$. Surf 2 (Fig. S1d) features a micro/nanostructure with dual textures composed of protrusions less than $50\ \mu\text{m}$ in diameter overlaid with nanofibers that are $1\ \mu\text{m}$ long and $200\ \text{nm}$ wide. Its unique bionic porous structure, combined with the enrichment of low-surface-energy functional groups ($-\text{CF}_3$), reduces its surface energy to the lowest among all surfaces (approximately $6.7\ \text{mN/m}$). However, the micro/nanostructure increases the surface roughness to over $3\ \mu\text{m}$, and the WCA reaches 150.82° , with air pockets present at the solid-liquid interface, indicative of the

Cassie state. In summary, the fabrication of surfaces with these distinct characteristics provides an experimental basis for studying the effects of homogeneous wettability surfaces and wettability-patterned surfaces on water flow behavior.

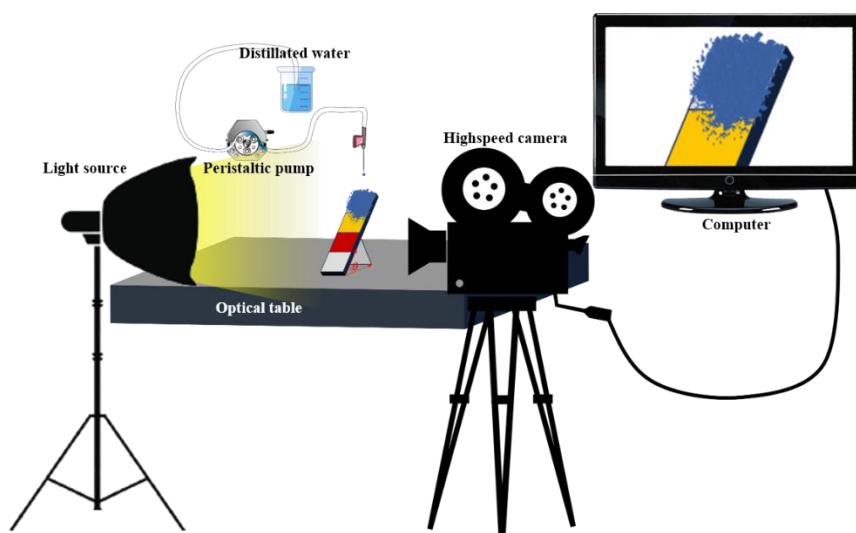


Fig. S3 Diagram of the experimental setup for water flow on wettability-patterned surfaces.

The main components of the experimental system for water flow on wettability-patterned surfaces include: a peristaltic pump for droplet transportation, a droplet generator with a needle, surface samples, an adjustable-angle sample holder, a position-adjustable platform to support the surface under impact, a digital camera or high-speed camera for image acquisition, a flicker-free light source for illumination, and a computer for recording and storing images. A schematic diagram of the experimental setup is shown in Fig. S2.

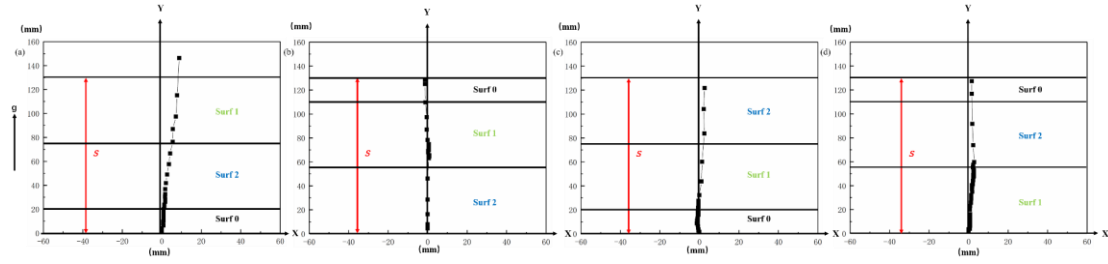


Fig. S4 Flow trajectories of water on wettability-patterned surfaces with different combinations. Ordered wettability-patterned surfaces (a-b). Disordered wettability-patterned surfaces (c-d).

By establishing an X-Y coordinate system parallel to the interface, the Y-axis is defined as the positive direction from the starting point to the endpoint of the water flow, while the X-axis is perpendicular to the flow direction, used to describe the deviation of the water flow on the wettability-patterned surface (as shown in Fig. S4). The experiment recorded the position of the water flow frame by frame, displaying the trajectory distribution in the X-Y plane.

Experimental results indicate that water flow along the positive Y-axis is not perfectly linear but exhibits varying degrees of deviation along the X-axis. This deviation is closely related to the microstructure and energy distribution of the surface. For instance, on the bare aluminum substrate, groove structures significantly influence the flow direction, causing the water to preferentially follow the groove orientation. Meanwhile, protruding regions on the surface force the water flow to bypass these areas, resulting in lateral deviation. The occurrence of this deviation demonstrates the critical role of surface microstructure and energy distribution in regulating the direction of water flow.

In summary, the degree of water flow deviation is closely related to the total flow time; shorter total flow times correspond to larger deviations. However, the overall deviation is relatively small compared to the primary flow direction along the Y-axis, and thus, the impact of deviation can be neglected. Water flow can be approximated as linear motion down the inclined surface. Based on this assumption, studying the instantaneous velocity of water flow is scientifically reasonable and provides an analytical foundation for further investigation of how the "Interfacial Barrier" regulates flow behavior.



Fig. S5 Macroscopic views of water flow on wettability-patterned surfaces. Ordered wettability-patterned surfaces (a-b). Disordered wettability-patterned surfaces (c-d).

By studying the macroscopic flow modes of water on different wettability-patterned surfaces, it was observed that water tends to retain its inherent flow mode within each wettability region. On Surf 0, water maintains the spindle-shaped sliding mode characteristic of hydrophilic surfaces; on Surf 1, it retains the spindle-shaped sliding mode typical of hydrophobic surfaces; and on Surf 2, it exhibits the ball-shaped rolling mode. As shown in Fig. S5a, water flow on the patterned surface with a gradually increasing wettability interfaces crossing relatively quickly, with a smaller "Interfacial Barrier" effect. In contrast, as shown in Fig. S5c, the disordered hydrophilic-superhydrophobic-hydrophobic patterned surface exhibits the second shortest total flow time, but water must overcome a larger energy barrier to transition

from the spindle-shaped sliding mode to the ball-shaped rolling mode. As shown in Figure S5b, on the surface with a gradually decreasing wettability, the average flow velocity is suppressed, and the flow mode transitions from ball-shaped rolling to spindle-shaped sliding on the hydrophobic surface and eventually reverts to spindle-shaped sliding on the hydrophilic surface, resulting in a longer total flow time. The disordered hydrophobic-superhydrophobic-hydrophilic patterned surface exhibits the slowest mode transition (Fig. S5d) and experiences a more pronounced "Interfacial Barrier" effect, with crossing times of approximately 880 ms. In summary, the flow mode of water is primarily influenced by wettability. Additionally, for orderly patterned wettability surfaces, the difference between forward and reverse flow times is much smaller compared to disordered wettability surfaces. This difference is mainly determined by the magnitude and direction of the wettability gradient.

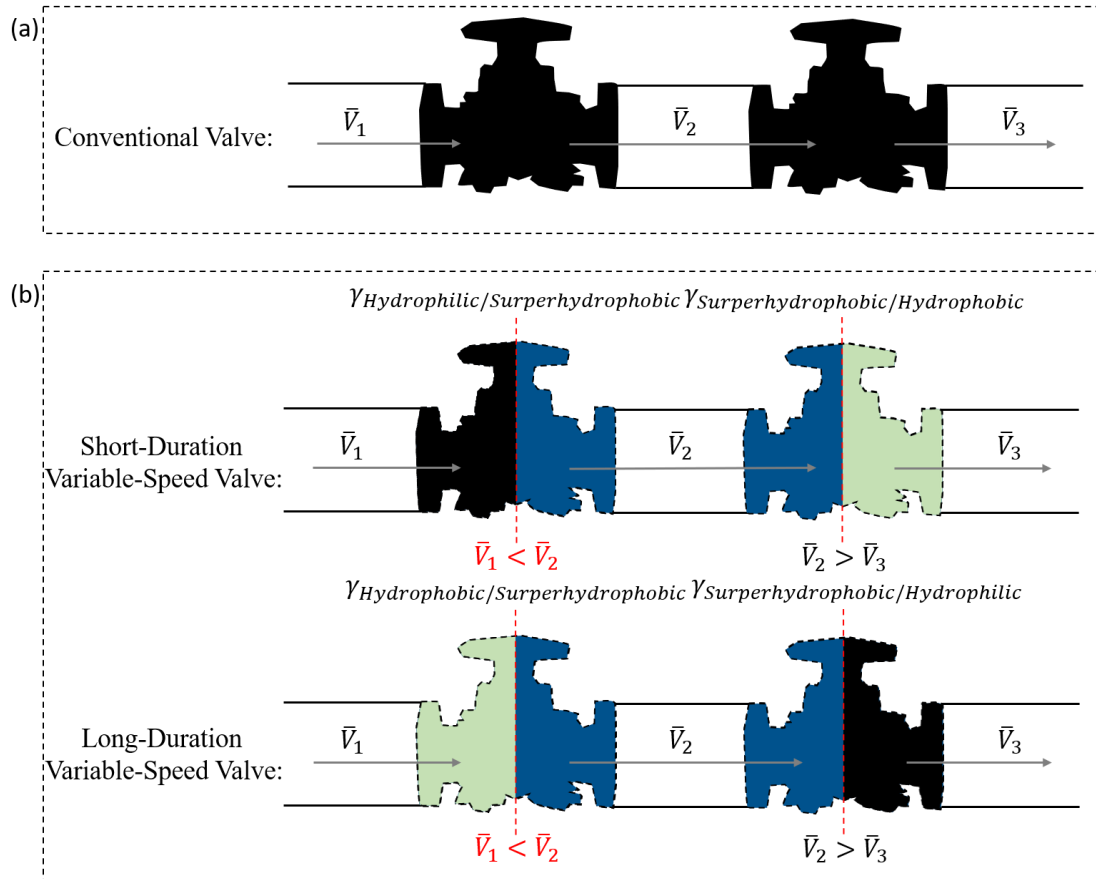


Fig. S6 Schematic of a traditional valve (a) and innovative variable-speed valves (b).

Using the "Interfacial Barrier" effect observed on disordered wettability surfaces, a "Smart" valve capable of autonomously regulating the average flow velocity of water was designed, as illustrated in Fig. S6. Traditional valves (Fig. S6a) require external energy input, such as adjusting pipe diameter, to regulate flow velocity. In contrast, the "Smart" valve (Fig. S6b) leverages wettability gradients and the "Interfacial Barrier" effect to achieve two-stage flow velocity regulation without the need for additional energy input.

Specifically, when water flows from the hydrophilic segment into the superhydrophobic segment (short-duration variable-speed valve), the flow velocity autonomously increases from \bar{V}_1 to \bar{V}_2 . Subsequently, after crossing the interface $\gamma_{Superhydrophobic/Hydrophilic}$, the velocity decreases from \bar{V}_2 to \bar{V}_3 . Similarly, when water flows from the hydrophobic segment into the superhydrophobic segment (long-duration variable-speed valve), the velocity autonomously increases from \bar{V}_1 to \bar{V}_2 . After crossing the interface $\gamma_{Superhydrophobic/Hydrophilic}$, \bar{V}_2 further decreases to \bar{V}_3 .

This is equivalent to water flowing in the opposite direction in short-duration variable-speed valve, but the total flow time in short-duration variable-speed valve is significantly shorter than in long-duration variable-speed valve. This phenomenon demonstrates that by precisely controlling wettability differences, effective regulation of regional average flow velocity and flexible adjustment of total flow time can be achieved without additional energy input or manual operation. This design fully utilizes the advantages of the "Interfacial Barrier" effect and dynamic wetting regulation, achieving low-energy, high-efficiency flow velocity control while simplifying the complex structural design of traditional mechanical valves and eliminating dependence on external energy input. It provides an innovative and efficient solution for future fluid processing scenarios requiring rapid response.

Hydrophobic increase direction

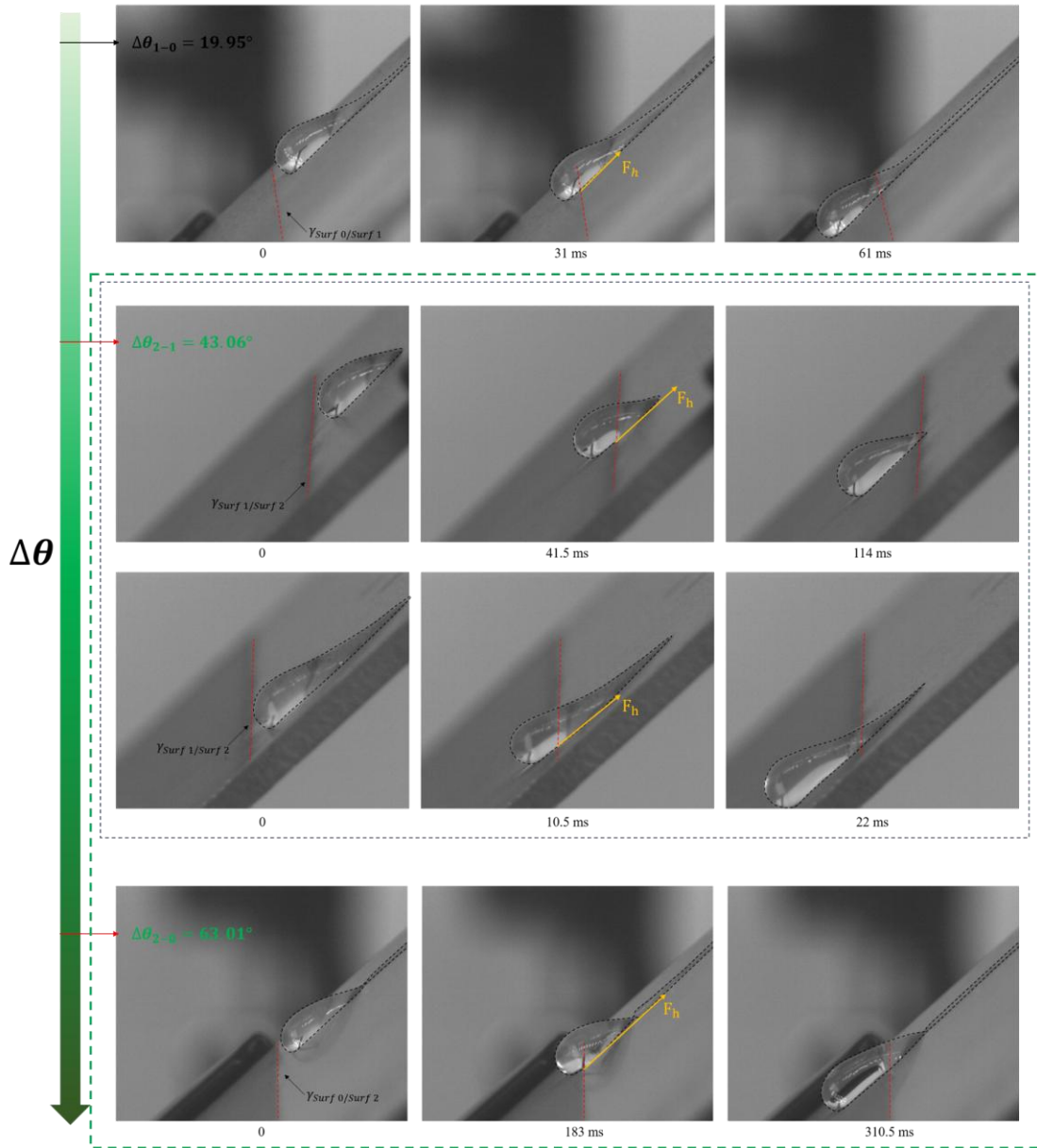


Fig. S7 High-speed images capturing water flow across an inclined surface with a rising hydrophobicity gradient.

As shown in Fig. S7, the behavior of water flow crossing interfaces along the direction of increasing hydrophobicity was monitored using a high-speed camera at 2000 fps. When the water flow crosses the $\gamma_{surf\ 0/surf\ 1}$ interface, it adopts the spindle-shaped sliding mode, with no significant change in its flow behavior before and after crossing the interface. However, when crossing the $\gamma_{surf\ 1/surf\ 2}$ or $\gamma_{surf\ 0/surf\ 2}$ interfaces, the flow behavior undergoes a uniform change, appearing to "climb a step"

to cross the interface. Specifically, the maximum height of the spindle increases after crossing the interface, and as hydrophobicity increases, the advancing and receding contact angles of the droplets also increase, giving the water flow a "step-climbing" effect.

Hydrophobic decrease direction

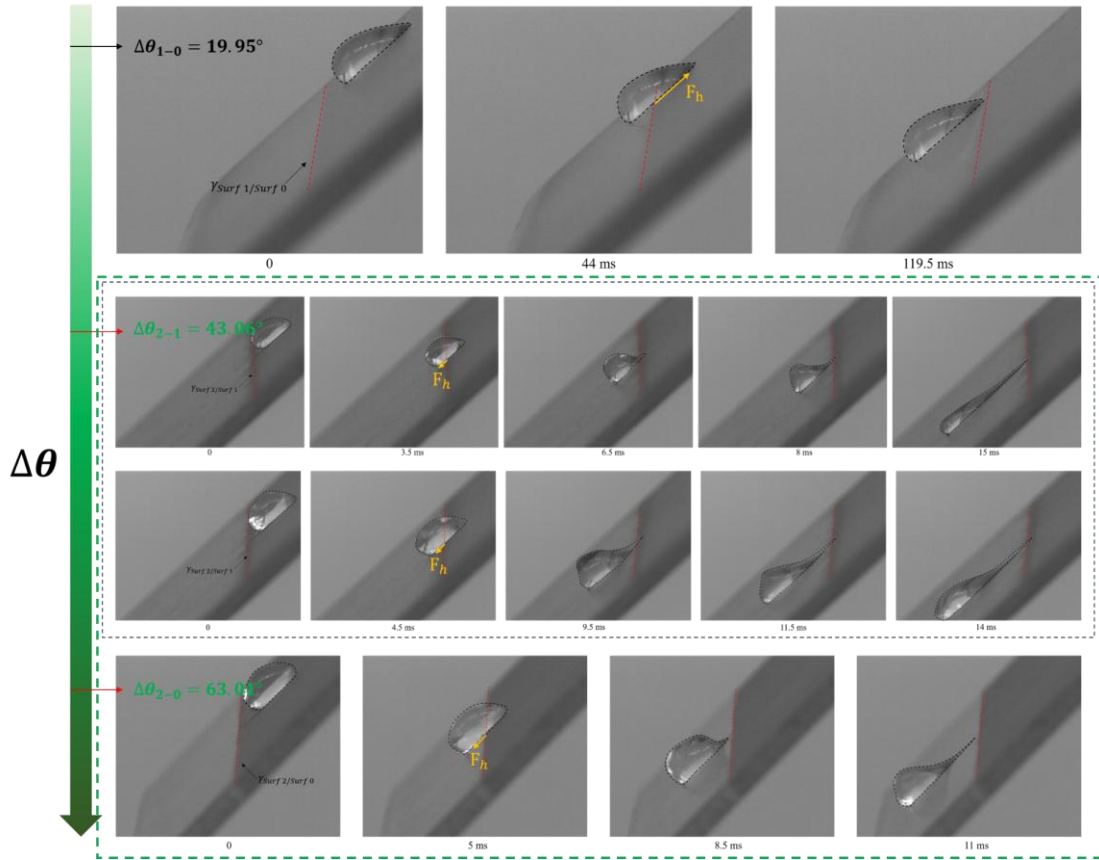


Fig. S8 High-speed images capturing water flow on an inclined surface across a decreasing hydrophobicity gradient.

As shown in Fig. S8, the behavior of water flow crossing interfaces along the direction of decreasing hydrophobicity was monitored using a high-speed camera at 2000 fps. When the water flow crosses the $\gamma_{Surf\ 1/Surf\ 0}$ interface, it maintains the spindle-shaped sliding mode, with no significant change in its flow behavior before and after crossing the interface. However, when crossing the $\gamma_{Surf\ 2/Surf\ 1}$ or $\gamma_{Surf\ 2/Surf\ 0}$ interfaces, the flow behavior undergoes a uniform transformation. The water flow approaches the interface in a ball-shaped rolling mode, deforms into a "parallelogram" shape upon contact with the interface, transitions into a "whale shape" after crossing, and finally restores to the spindle-shaped sliding mode.

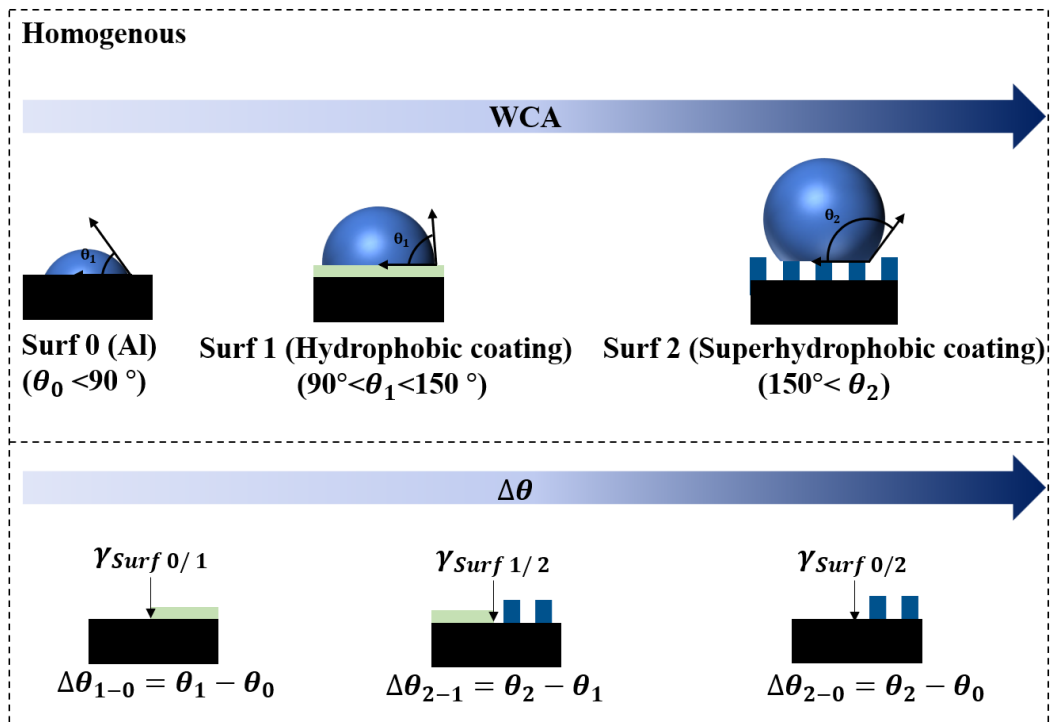


Fig. S9 Schematic design for microscopic droplet impact analysis on a flat surface. Here, $\Delta\theta$ represents the static contact angle difference between the two sides of the interface.

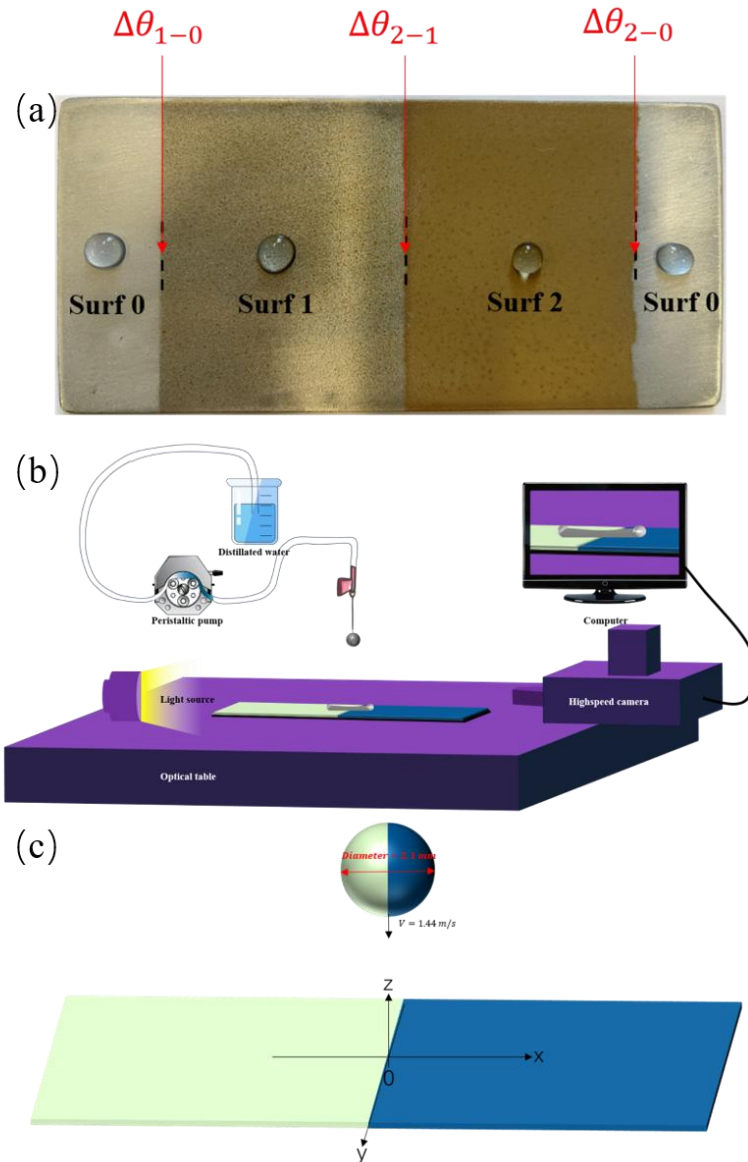


Fig. S10 Photograph of the wettability-patterned surface (a), experimental setup (b), and schematic of the analysis method (c) for single droplet impact.

The wettability-patterned surfaces comprising combinations of Surf 0, Surf 1, and Surf 2 were designed and prepared on a bare aluminum substrate using the overlay spray-coating method, as shown in Fig. S10a.

The experimental system for single droplet impact on wettability-patterned surfaces consists of key components including a peristaltic pump for droplet transportation, a droplet generator with a needle, samples, a position-adjustable platform to support the impacted surface, a high-speed camera for image capture, a

flicker-free lamp for high-speed imaging illumination, and a computer for recording and storing the captured images. The experimental setup is shown in Fig. S10b.

To more accurately quantify the dynamic wetting process of droplets impacting wettability-patterned surfaces, a coordinate system was established. The direction orthogonal to the interface line was defined as the x-axis, with the direction of increasing hydrophobicity set as positive. The impact center was designated as the origin of the x-y coordinate system, the interface line as the y-axis, with the direction toward the camera set as positive for the y-axis. The z-axis was defined as perpendicular to the xy-plane, with the direction away from the surface as positive, as shown in Fig. S10c.

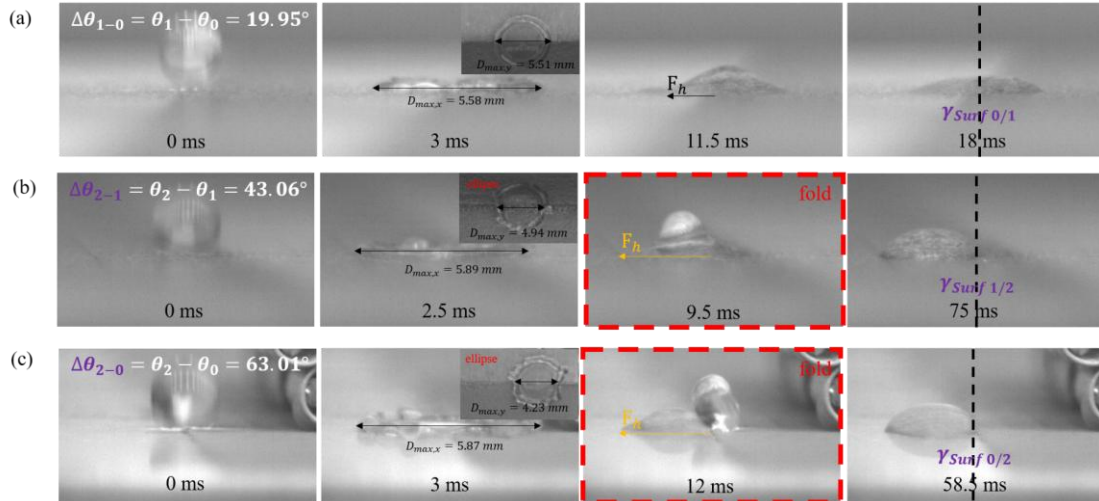


Fig. S11 High-speed delayed photos of droplet impact on wettability-patterned surfaces at room temperature (25°C) with $We=60$. Droplet impact on the $\gamma_{surf\ 0/1}$ interface (a), $\gamma_{surf\ 1/2}$ interface (b), and $\gamma_{surf\ 0/2}$ interface (c). $We = \rho U_0^2 D_0 / \gamma_{LV}$, where ρ is the density of water, U_0 is the droplet impact velocity on the surface, D_0 is the droplet diameter.

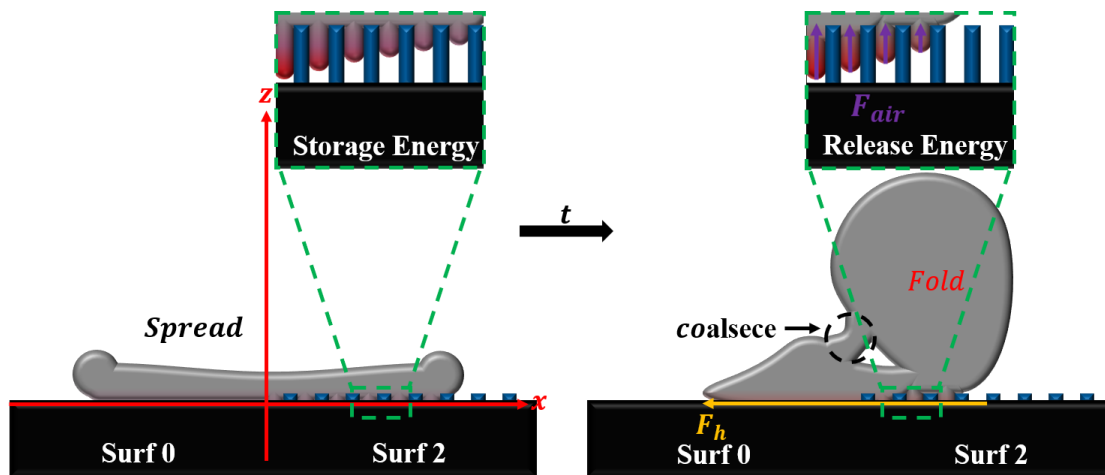


Fig. S12 Schematic illustration of the dynamic wetting behavior of "Droplet Folding" at the $\gamma_{surf\ 0/2}$ interface.

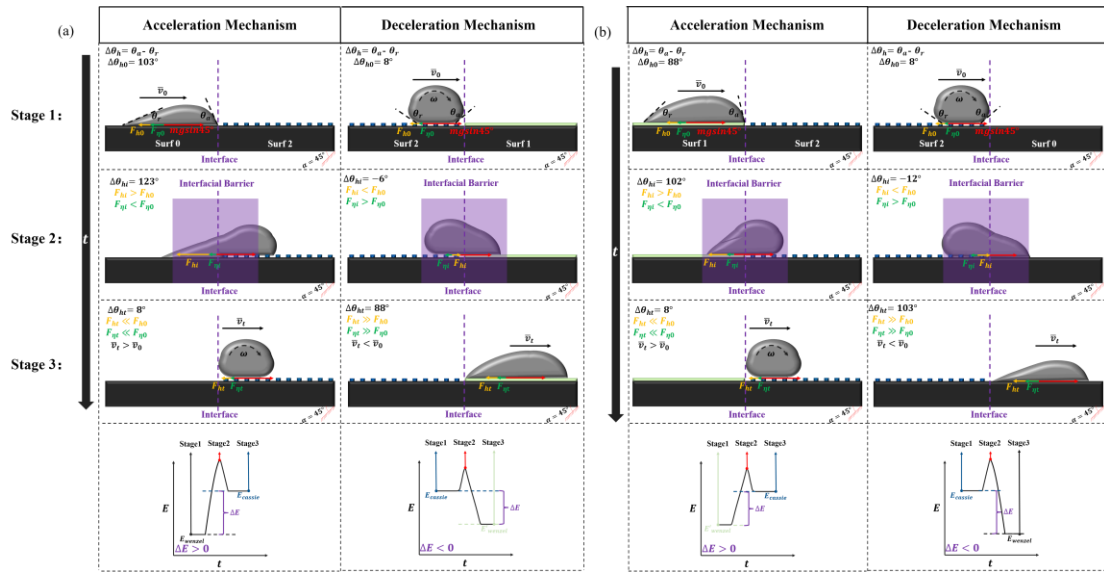


Fig. S13 Force analysis diagrams for the disordered wettability-patterned surfaces: Pattern III

(a); Pattern IV (b).

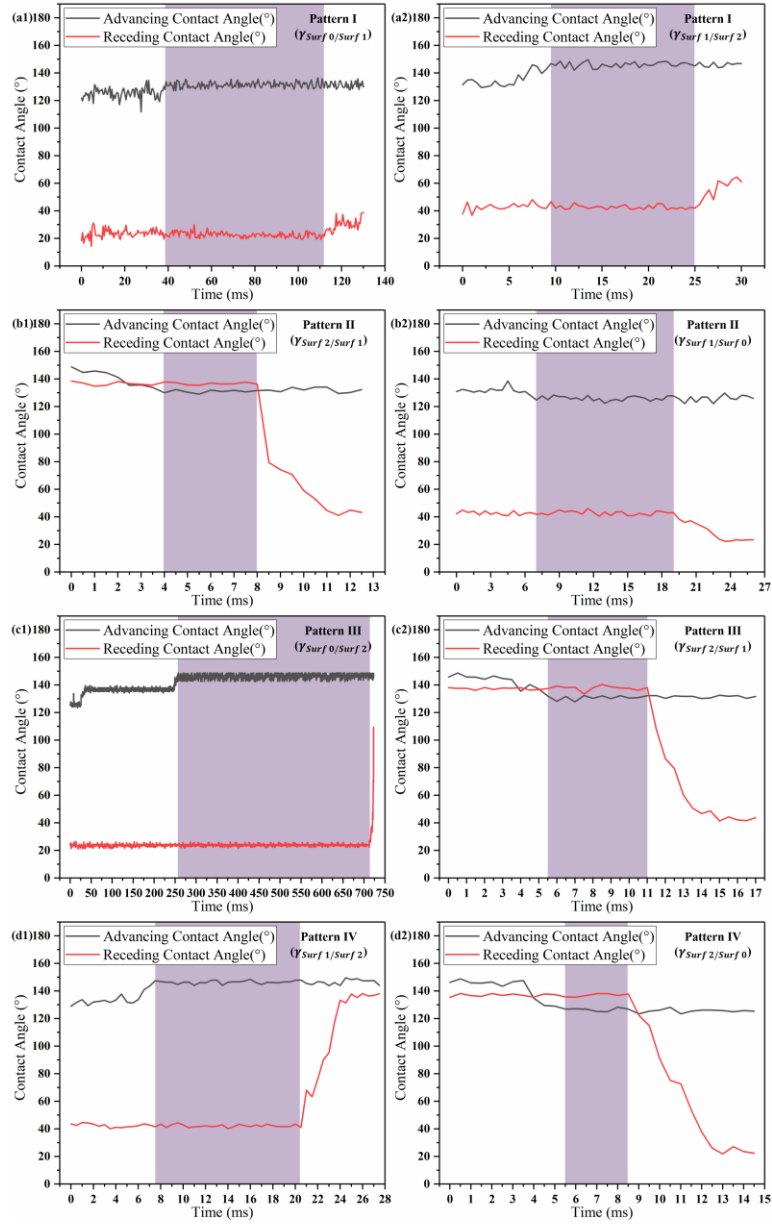


Fig. S14 Dynamic contact angle variations on four wettability-patterned surfaces: Pattern I (a1-2); Pattern II (b1-2); Pattern III (c1-2); Pattern IV (d1-2).

Table S1 Characteristics of homogenous wettability surfaces.

Number	Sample	Roughness (μm)	Thickness (μm)	WCA ($^\circ$)	WSA ($^\circ$)	Surface Energy (mN/m)
1	Surf 0	1.2	\	78.58	\	114.55
2	Surf 1	3	21.9	98.53	\	23.94
3	Surf 2	3.13	33.1	150.82	5	6.7

The surfaces used in this study were based on the team's previous research on constructing bioinspired superhydrophobic surfaces and investigating droplet impact behavior as well as anti-icing behavior at the droplet-solid interface. These surfaces were incorporated into a bioinspired self-cleaning coating system, with characteristic parameters listed in Table S1. First, regarding coating thickness, all two coatings, except for the substrate, had thicknesses of several tens of micrometers. Additionally, the surface roughness of Surf 0 was approximately one micrometer, allowing them to be approximated as smooth surfaces in this study. The contact angles of the three surfaces increase sequentially, with Surf 2 exhibiting a rolling angle and demonstrating excellent water-shedding performance. From the perspective of surface energy, the bare aluminum substrate had a significantly higher surface energy compared to the other two coatings. This difference in surface energy greatly amplified the wettability differences, leading to distinct dynamic wetting behaviors on the three surfaces.

Table S2 Advancing and Receding Contact Angles of Homogeneous Wettability Surfaces.

Number	Sample	θ_a (°)	θ_r (°)
1	Surf 0	125.7	23.0
2	Surf 1	131.6	43.4
3	Surf 2	146.0	137.6